International Journal of Thermophysics, Vol. 12, No. 6, 1991

Thermodynamic Analysis of Stable and Metastable Carbides in the Mn–V–C System and Predicted Phase Diagram

A. Fernández Guillermet[1] and W. Huang[2]

Received March 26, 1991

The thermodynamic properties of the Mn–V–C system are not known from experiments, and there is a need for information on the stability of the various phases and the Mn–V–C phase diagram. This kind of information has been obtained by us. Our approach combines the methods of phenomenological modeling and extrapolation from the lower-order systems, which have been developed in the so-called CALPHAD (i.e., CALculation of PHAse Diagrams) work, with predictions of unknown thermodynamic quantities. The predictions are based on regularities in bonding properties and vibrational entropy of 3d-transition metal carbides. By using predicted Gibbs energy functions as input information in the Hillert–Staffansson "two-sublattice" phenomenological model, we take into account the substitution of Mn for V in all carbide phases. Our results are summarized in tables of thermodynamic parameters, calculated isothermal sections of the phase diagram, and the liquidus surface.

KEY WORDS: carbides; enthalpy; entropy; manganese compounds; metastable phases; phase diagrams; vanadium compounds.

1. INTRODUCTION

The study of the thermodynamic properties of the transition-metal alloys and compounds is a subject of considerable practical and theoretical interest. Accurate thermodynamic information forms the basis of the so-called CALPHAD (i.e. CALculation of PHAse Diagrams) approach

[1] Consejo Nacional de Investigaciones Científicas y Técnicas, Centro Atómico Bariloche, 8400 San Carlos de Bariloche, Argentina.

[2] Division of Physical Metallurgy, Royal Institute of Technology, S-10044 Stockholm, Sweden.

0195-928X/91/1100-1077$06.50/0

to phase diagrams of multicomponent alloy systems. In this approach, pioneered by Kaufman [1, 2], one searches for a consistent thermodynamic description, based on modeling the Gibbs energy (G) functions of the various phases in the multicomponent system, making use of the descriptions of the lower-order systems, e.g., binaries and ternaries.

The models used in current CALPHAD work are phenomenological and contain parameters which are fitted to experimental information on the phase diagram and thermochemical properties. In particular, some of the adjustable parameters involved in the so-called compound-energy model [3] of multicomponent solid solution phases represent the Gibbs energy of compounds which are not stable in the system. Since the experimental information necessary to determine the model parameters accurately is often uncertain, scarce, or lacking, there is a strong interest in the development of methods for predicting the Gibbs energy of those metastable compounds.

Miedema's formula [4] has been very successful in accounting for the enthalpy of formation of various groups of compounds, but it does not treat the entropy part of G, which is important in a consideration of the phase equilibria at high temperatures. The problem of estimating G at high temperatures led Fernández Guillermet and Grimvall [5] to a systematic study of the thermodynamics of various 3d-transition metal compounds. They have reported various correlations which allowed the estimation of, e.g., the room temperature entropy and the enthalpy of formation of various stable carbides, nitrides, and oxides. Besides, their correlations have been used in studying the properties of various stable and metastable phases, e.g., a phase with the (cF8) NaCl structure in the Cr–C system [6], the metastable (cF8) NaCl-structure phase "NiN" and other nitride phases in the Ni–N system [7], and the metastable (oP16) ("cementite"-structure) phase Cr_3C in the Cr–C system [8].

The purpose of the present work is to go one step further and combine the estimation procedures introduced in Refs. 5–8 with the methods of analysis and extrapolation developed in CALPHAD work, to gain information on the high-temperature thermodynamics of a ternary system which is not known from experiments, the Mn–V–C system. This study is part of a research program aimed at treating the Fe–Mn–V–C system which is currently carried on by one of us (W.H.). Previous publications by Huang have dealt with the treatment of the binary sides of this ternary system, the Mn–C [9], V–C [10], and Mn–V [11] systems. The remainder of the present paper is organized as follows. In Section 2 we present the models for the Gibbs energy of the various phases in the ternary system, and in Section 3 we explain the procedure for evaluation of model parameters. Sections 4 and 5 are devoted to the so-called "lattice stabilities" and the

excess Gibbs energy of carbide phases, respectively. In Section 6 we calculate and discuss the Mn–V–C phase diagram, and in Section 7 we summarize our work.

2. THERMODYNAMIC MODELING

2.1. Nonmagnetic Gibbs Energy of Solid Solution Phases

The Gibbs energy of the bcc, fcc, hcp, α-Mn, and β-Mn solid solution phases was described by resolving it into a magnetic (ΔG_m^{mg}) and a nonmagnetic contribution. The magnetic contribution was described by Hillert and Jarl's [12] modification of the model proposed by Inden [13], whereas the nonmagnetic contribution was described by the two-sublattice [14] version of the compound-energy model [3]. Mn and V were assumed to occupy the first sublattice, whereas C atoms and vacant interstitial sites (Va) were assumed to substitute for each other in the second one. The bcc, fcc, hcp, α-Mn, and β-Mn solid solution phases were represented in the present work by the two-sublattice model $(Mn, V)_1 (C, Va)_c$, and their Gibbs energy per mole of formula units was described by the following expression:

$$\begin{aligned} G_m^{\phi} = {} & y_{Mn}\, y_{Va}\, {}^0G^{\phi}_{Mn:Va} + y_V\, y_{Va}\, {}^0G^{\phi}_{V:Va} + y_{Mn}\, y_C\, {}^0G^{\phi}_{Mn:C} + y_V\, y_C\, {}^0G^{\phi}_{V:C} \\ & + RT[(y_{Mn} \ln y_{Mn} + y_V \ln y_V) \\ & + c(y_C \ln y_C + y_{Va} \ln y_{Va})] + {}^EG_m^{\phi} + \Delta G_m^{mg,\phi} \end{aligned} \tag{1}$$

The variable $y_i (i = C, Mn, V, Va)$ is the so-called [15] site fraction of component i in its sublattice. The parameter ${}^0G^{\phi}_{i:Va}$ is the Gibbs energy of pure component i in a nonmagnetic state with the structure ϕ, and ${}^0G^{\phi}_{i:C}$ is the Gibbs energy of a state where all the interstitial sites are filled with C. The symbol c denotes the number of interstitial sites per metallic atom. For the bcc structure $c = 3$, and for the fcc structure $c = 1$. The hcp structure was treated by adopting $c = 0.5$, and for the α-Mn and β-Mn structure we adopted $c = 1$. All the ${}^0G^{\phi}_{i:Va}$ values were referred to the enthalpy of a special standard state recommended by the SGTE (Scientific Group Thermodata Europe) organization [16]. This state, denoted by the superscript SER (Stable Element Reference), is defined as the stable state at 298.15 K and 0.1 MPa. The necessary information on ${}^0G^{\phi}_{Mn:Va}$ was taken from Ref. 17, and information on ${}^0G^{\phi}_{V:Va}$ from Refs. 18 and 19. The ${}^0G^{\phi}_{Mn:C}$ quantities, which originate in the Mn–C system, were taken from Ref. 9, whereas the ${}^0G^{\phi}_{V:C}$ quantities, which originate in the V–C system, were

taken from Ref. 10. The term ${}^{E}G_{m}^{\phi}$ in Eq. (1) is the excess Gibbs energy term. It was expressed as follows:

$$\begin{aligned} {}^{E}G_{m}^{\phi} = {} & y_{Mn}\, y_{V}(y_{C} L^{\phi}_{Mn,V:C} + y_{Va} L^{\phi}_{Mn,V:Va}) \\ & + y_{Va}\, y_{C}(y_{Mn} L^{\phi}_{Mn:C,Va} + y_{V} L^{\phi}_{V:C,Va}) \end{aligned} \tag{2}$$

where the L parameters are composition dependent according to the so-called Redlich–Kister [20] phenomenological power series, i.e.,

$$L^{\phi}_{Mn,V:j} = \sum_{k=0}^{n} {}^{(k)}L^{\phi}_{Mn,V:j}(y_{Mn} - y_{V})^{k} \tag{3}$$

with $j = C$ or Va, and

$$L^{\phi}_{i:C,Va} = \sum_{k=0}^{n} {}^{(k)}L^{\phi}_{i:C,Va}(y_{C} - y_{Va})^{k} \tag{4}$$

with $i = Mn$ or V.

The quantities ${}^{(k)}L^{\phi}$ are, in general, functions of temperature. In Eqs. (2)–(4) the comma separates components that interact in the same sublattice, and the colon separates components in different sublattices. The parameters $L^{\phi}_{Mn:C,Va}$ were taken from Ref. 9, and the quantities $L^{\phi}_{V:C,Va}$ from Ref. 10. The parameters $L^{\phi}_{Mn,V:Va}$ which come from the Mn–V system were taken from Ref. 11, whereas the quantities $L^{\phi}_{Mn,V:C}$ which originate in the Mn–V–C system are discussed in Section 5.

2.2. The Magnetic Contribution

The last term in Eq. (1), which is the magnetic contribution to the Gibbs energy, is given by the expression

$$\Delta G_{m}^{mg,\phi} = RT \ln(\beta^{\phi} + 1) f^{\phi}(\tau) \tag{5}$$

where β^{ϕ} is a composition-dependent parameter related to the total magnetic entropy, i.e., the quantity $\Delta S_{m}^{mg,\phi}(\infty) - \Delta S_{m}^{mg,\phi}(0)$, as follows:

$$\Delta S_{m}^{mg,\phi}(\infty) - \Delta S_{m}^{mg,\phi}(0) = R \ln(\beta^{\phi} + 1) \tag{6}$$

τ is defined as T/T_{C}^{ϕ}, where T_{C}^{ϕ} is the critical temperature for magnetic ordering of the structure ϕ at a given composition, i.e., the Curie temperature (T_{C}) for ferromagnetic ordering and the Néel temperature (T_{N}) for antiferromagnetic ordering, and $f^{\phi}(\tau)$ represents the polynomial proposed by Hillert and Jarl [12]. When applying the model to alloys, the

composition dependence of the quantities β^ϕ and T_C^ϕ has to be accounted for. This was done by adopting the following phenomenological expression:

$$\begin{aligned} I^\phi = {} & y_{Mn}\, y_{Va}\, {}^0I^\phi_{Mn:Va} + y_{Mn}\, y_C\, {}^0I^\phi_{Mn:C} + y_V\, y_{Va}\, {}^0I^\phi_{V:Va} + y_V\, y_C\, {}^0I^\phi_{V:C} \\ & + y_{Mn}\, y_V (y_C I^\phi_{Mn,V:C} + y_{Va} I^\phi_{Mn,V:Va}) \\ & + y_C\, y_{Va} (y_{Mn} I^\phi_{Mn:C,Va} + y_V I^\phi_{V:C,Va}) \end{aligned} \tag{7}$$

I stands for T_C or β. The $I^\phi_{Mn:Va}$ quantities, which represent the magnetic contribution to G_m of the solid phases of Mn, were taken from Ref. 17 and the remaining parameters were set equal to zero.

2.3. Carbides

2.3.1. Cubic (MeC) and Hexagonal (Me_2C) Carbides

The MeC (cF8) NaCl-structure carbide phase is stable in the V–C system [21], with a range of homogeneity. The MeC carbide may be considered as derived from the interstitial solution of C in the metastable fcc (cF4) phase of V, by filling up with carbon atoms all octahedral interstitial sites. This fact was taken into account in Ref. 10, and the properties of the NaCl structure phase VC were described as the carbon-rich end of the Gibbs energy function for the fcc interstitial solution, which was represented by the two-sublattice model $(V)_1\,(C, Va)_1$. The same type of model was applied in Ref. 9 to treat the fcc phase, which is stable in the Mn–C system, i.e., $(Mn)_1\,(C, Va)_1$. As a natural generalization we treat the properties of the ternary phase extending between the V-rich (cF8) structure and the Mn-rich (cF4) fcc phase by the two-sublattice model $(Mn, V)_1\,(C, Va)_1$. Its G_m function is described by Eq. (1) with $c = 1$, and the necessary information taken from the references given in Section 2.

In a similar way, the two-sublattice model $(Mn, V)(C, Va)_{0.5}$ was adopted to treat the properties of the hexagonal Me_2C (hP3) carbide structure in the ternary system, which originates in the V_2C phase of the V–C system [21]

2.3.2. Complex Carbides: Me_3C_2, Me_7C_3, Me_5C_2, and Me_3C

Various complex carbide phases were treated in the present work. Among them Me_7C_3(oP40), Me_5C_2 (mC28), and Me_3C(oP16) originate in the Mn–C system [9]. The carbide Me_3C_2 (hR20) originates in the V–C system and represents the observed composition of a carbide with the ideal formula "V_4C_3"; see Ref. 21. No experimental information on the

solubility of V in the Mn-rich carbides or Mn in the V-rich carbides was found in the literature, and the possibility was considered by us of setting those solubilities at zero, i.e., treating these carbides as true binary phases. However, preliminary calculations revealed a significant solubility in the ternary cubic or hexagonal carbides, and it was considered more realistic to allow Mn and V atoms to substitute for each other also in the complex carbides. The carbides Me_7C_3, Me_5C_2, and Me_3C were thus assumed to be stoichiometric with respect to carbon and were represented by the two-sublattice model $(Mn, V)_b C_c$. Their Gibbs energy per mole of formula units was expressed as

$$G_m^{\phi} = y_{Mn}\,{}^0G_{Mn:C}^{\phi} + y_V\,{}^0G_{V:C}^{\phi} + bRT(y_{Mn}\ln y_{Mn} + y_V \ln y_V) + {}^EG_m^{\phi} \quad (8)$$

The parameters ${}^0G_{V:C}^{Me_3C_2}$, ${}^0G_{Mn:C}^{Me_7C_3}$, ${}^0G_{Mn:C}^{Me_5C_2}$, and ${}^0G_{Mn:C}^{Me_3C}$ represent the Gibbs energy functions for the stable carbides in the V–C and Mn–C systems. They were taken directly from Refs. 9 and 10. The parameters ${}^0G_{Mn:C}^{Me_3C_2}$, ${}^0G_{V:C}^{Me_7C_3}$, ${}^0G_{V:C}^{Me_5C_2}$, and ${}^0G_{V:C}^{Me_3C}$ represent the Gibbs energy functions for the metastable carbides Mn_3C_2, V_7C_3, V_5C_2, and V_3C, respectively. These quantities were expressed in terms of the enthalpy of the elements in their reference states as

$${}^0G_{Mn:C}^{Me_3C_2} = 3H_{Mn}^{SER} + 2H_C^{SER} + \Delta^0G_{Mn_3C_2} \quad (9)$$

$${}^0G_{V:C}^{Me_bC_c} = bH_V^{SER} + cH_C^{SER} + \Delta^0G_{V_bC_c} \quad (10)$$

and the Gibbs energy differences $\Delta^0G_{Mn_3C_2}$, $\Delta^0G_{V_7C_3}$, $\Delta^0G_{V_5C_2}$, and $\Delta^0G_{V_3C}$ were treated as functions of temperature in a way described in Section 4. The information on the properties of graphite, which is necessary for applying Eqs. (9) and (10), was taken from Ref. 22. The last term in Eq. (8) is the excess Gibbs energy. It was treated using the regular solution approximation,

$${}^EG_m^{\phi} = y_V\,y_{Mn}\,{}^0L_{Mn,V:C}^{\phi} \quad (11)$$

The interaction parameter ${}^0L_{Mn,V:C}^{\phi}$ is discussed in Section 5.

2.3.3. $Me_{23}C_6$ Carbide

The $Me_{23}C_6$ (cF116) carbide phase, which originates in the Mn–C system [9], was also treated as stoichiometric with respect to carbon. However, instead of the simple two-sublattice model $(Mn, V)_{23}C_6$, a more elaborate representation was adopted. A three-sublattice treatment has been previously proposed for the $Me_{23}C_6$ carbide in the Fe–Cr–C system [23], from a consideration of crystallographic data, and from infor-

mation on the homogeneity range of this phase in higher-order systems, e.g., the Fe–Cr–W–C [24] and Fe–Cr–Mo–C [25] systems. That model was accepted by us, in order to make the present treatment of the Mn–V–C compatible with those previous works. Accordingly, we represented the $Me_{23}C_6$ carbide by the three-sublattice model $(Mn, V)_{20}(Mn, V)_3 C_6$ and described its Gibbs energy per mole of formula units using the expression,

$$\begin{aligned} G_m^{Me_{23}C_6} = {} & y_{Mn}^1 y_{Mn}^2 {}^0G_{Mn:Mn:C}^{Me_{23}C_6} + y_{Mn}^1 y_V^2 {}^0G_{Mn:V:C}^{Me_{23}C_6} \\ & + y_V^1 y_{Mn}^2 {}^0G_{V:Mn:C}^{Me_{23}C_6} + y_V^1 y_V^2 {}^0G_{V:V:C}^{Me_{23}C_6} \\ & + RT[20(y_{Mn}^1 \ln y_{Mn}^1 + y_V^1 \ln y_V^1) \\ & + 3(y_{Mn}^2 \ln y_{Mn}^2 + y_V^2 \ln y_V^2)] + {}^E G_m^{Me_{23}C_6} \end{aligned} \tag{12}$$

where y_{Me}^1 and y_{Me}^2 are the site fraction in the first and second sublattice, respectively. ${}^0G_{Mn:Mn:C}^{Me_{23}C_6}$ represents the Gibbs energy of $Mn_{20}Mn_3C_6$, i.e., the $Mn_{23}C_6$ carbide. It was directly taken from Ref. 9. ${}^0G_{V:V:C}^{Me_{23}C_6}$ represents the Gibbs energy of the $V_{20}V_3C_6$, i.e., the $V_{23}C_6$ carbide, which is metastable in the V–C system. It was expressed as

$${}^0G_{V:V:C}^{Me_{23}C_6} = 23H_V^{SER} + 6H_C^{SER} + \Delta^0G_{V_{23}C_6} \tag{13}$$

and the temperature-dependent quantity $\Delta^0G_{V_{23}C_6}$ was determined as described in Section 4. Finally, the parameters ${}^0G_{Mn:V:C}^{Me_{23}C_6}$ and ${}^0G_{V:Mn:C}^{Me_{23}C_6}$ correspond to the hypothetical ternary compounds $Mn_{20}V_3C_6$ and $V_{20}Mn_3C_6$. Because of the lack of information on these carbides we adopted a method previously applied in the Fe–Cr–C system [23] and approximated their Gibbs energy by the weighted average of the ${}^0G$ functions for $Mn_{23}C_6$ and $V_{23}C_6$, i.e., we assumed that

$$23{}^0G_{Mn:V:C}^{Me_{23}C_6} = 20{}^0G_{Mn:Mn:C}^{Me_{23}C_6} + 3{}^0G_{V:V:C}^{Me_{23}C_6} \tag{14}$$

$$23{}^0G_{V:Mn:C}^{Me_{23}C_6} = 20{}^0G_{V:V:C}^{Me_{23}C_6} + 3{}^0G_{Mn:Mn:C}^{Me_{23}C_6} \tag{15}$$

The last term in Eq. (12), which is the excess Gibbs energy for $Me_{23}C_6$, is considered in Section 5.

2.4. Sigma Phase

A tetragonal (tP30)-structure intermetallic phase, usually called the σ phase, is stable in the Mn–V system [11]. Its thermodynamic properties have been treated by applying the three-sublattice model $Mn_8V_4(Mn, V)_{18}$, and the reader is referred to Ref. 11 for details. Lacking experimental

information on the properties of the σ phase in the Mn–V–C system, we assumed that this phase does not dissolve any carbon and treated it as a binary phase, using the description assessed in Ref. 11.

2.5. Liquid Phase

The Gibbs energy of the liquid phase was described by applying a substitutional solution model, as follows:

$$\begin{aligned} G_m^L = {} & x_C {}^0G_C^L + x_{Mn} {}^0G_{Mn}^L + x_V {}^0G_V^L \\ & + RT(x_C \ln x_C + x_{Mn} \ln x_{Mn} + x_V \ln x_V) \\ & + x_C x_{Mn} L_{C,Mn} + x_C x_V L_{C,V} + x_{Mn} x_V L_{Mn,V} \end{aligned} \tag{16}$$

where ${}^0G_C^L$, ${}^0G_{Mn}^L$, and ${}^0G_V^L$ were taken from Refs. 22, 17, and 18, respectively. The interaction parameters, $L_{C,Mn}$, $L_{C,V}$, and $L_{Mn,V}$, which originate in the Mn–C [9], V–C [10], and Mn–V [11] systems, are in general composition dependent according to the Redlich–Kister [20] phenomenological power series. No ternary interaction term was included in Eq. (16) because of the lack of information.

3. PARAMETER EVALUATION PROCEDURE

Five thermodynamic model parameters were determined in the present work, $\Delta^0G_{Mn_3C_2}$, $\Delta^0G_{V_7C_3}$, $\Delta^0G_{V_5C_2}$, $\Delta^0G_{V_3C}$, and $\Delta^0G_{V_{23}C_6}$, which are related to the Gibbs energy of one metastable Mn carbide and four metastable V carbides, which are not known from experiments. They were determined by combining estimations of the high-temperature entropy of these carbides, based on the methods introduced in Refs. 5–8, with estimations of their enthalpy of formation, as discussed in Section 4.3. All fits to experimental or estimated information reported here were performed using ASSESSMENT, a computer program for the optimization of thermodynamic model parameters developed by Jansson [26]. The estimation of the Gibbs energy differences in Eqs. (9), (10), and (13), which are often referred to as "lattice stabilities" [1, 27] is discussed in the following section.

4. ANALYSIS OF LATTICE STABILITIES

4.1. General Considerations

Fernández Guillermet and Grimvall [5] have reported on various correlations between quantities related to the strength of chemical bonding

in 3d-transition metal carbides and the average number of valence electrons per atom, n_e. Of particular relevance for the present study is the correlation between the room-temperature enthalpy of formation per atom ($\Delta^0 H$) and n_e, and the correlation involving the characteristic energy E_S. This quantity, introduced in Ref. 5, was defined as

$$E_S = k_S \Omega^{2/3} \tag{17}$$

where Ω is the average volume per atom, and k_S is a quantity with the dimension of a force constant (i.e., force per length), which is related to the vibrational properties of the compound as follows:

$$k_S = M_{\text{eff}}(k_B \theta_S/\hbar)^2 \tag{18}$$

M_{eff} is the logarithmic average of the atomic masses, k_B is the Boltzmann constant, $\hbar = h/2\pi$ where h is Planck's constant, and θ_S is an "entropy Debye temperature," defined [28, 29] as the θ value which reproduces the experimental vibrational entropy per mole of atoms, S_{vib}, when inserted in the Debye model expression for the entropy, S_D,

$$S_{\text{vib}}(T) = S_D(\theta_S/T) \tag{19}$$

Previous analyses based on k_S of the vibrational entropy of transition metals [30] and their combinations with C, N, and B [28] revealed remarkable regularities. The new correlations involving $\Delta^0 H(\text{kJ} \cdot \text{mol}^{-1})$ and $E_S(\text{Ry})(1\text{Ry/atom} = 1312.8\ \text{kJ} \cdot \text{mol}^{-1})$ for 3d-transition metal carbides are given in Fig. 1. References to the sources of enthalpy and entropy information and a discussion of the data points for Mn compounds, which deviate from the general trend in Fig. 1b, have been given in Ref. 5 and are not repeated here.

4.2. Estimation of θ_S for Metastable Carbides

The correlation in Fig. 1a is now applied to predict the properties of the metastable carbides Mn_3C_2, V_7C_3, V_5C_2, V_3C, and $V_{23}C_6$. Our procedure is as follows. From the number of valence electrons of Mn, $n_e^{Mn} = 7e \cdot a^{-1}$, V, $n_e^V = 5e \cdot a^{-1}$, and C, $n_e^C = 4e \cdot a^{-1}$, we calculate n_e. For a carbide Me_bC_c, $n_e = (bn_e^{Me} + cn_e^C)/(b + c)$. Then, from the correlation in Fig. 1a we get E_S. From E_S and the experimental Ω we get k_S [Eq. (17)] and θ_S [Eq. (18)]. If experimental information on Ω of a compound is not available, we estimate it by relying on interpolations in Ω vs n_e plots between experimental data for phases with the same formula, as explained in Refs. 5 and 31. The Ω values obtained in this way are given in Table I.

Anharmonicity makes θ_S temperature dependent. When the vibrational entropy at high temperatures was needed in the study reported in Refs. 6 and 8, one let θ_S decrease with T, relying on the known behavior of the temperature dependence of θ_S for similar compounds. We have neglected such corrections here. We have also neglected nonvibrational contributions.

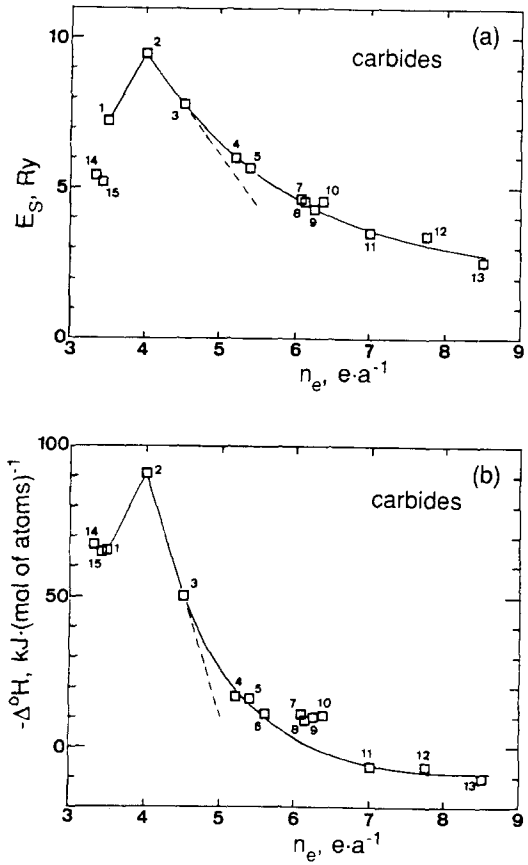

Fig. 1. (a) The entropy-related characteristic energy E_S, defined in Eq. (17), and (b) the negative enthalpy of formation of carbides at 298.15 K ($-\Delta^0H$), as a function of the average number of valence electrons per atom, n_e. The numbers refer to ScC(1), TiC(2), VC(3), Cr_3C_2(4), Cr_7C_3(5), $Cr_{23}C_6$(6), Mn_7C_3(7), Mn_5C_2(8), Mn_3C(9), $Mn_{23}C_6$(10), Fe_3C(11), Co_3C(12), Ni_3C(13), Sc_2C(14), and Sc_4C_3(15). The dashed lines refer to the (cF8) NaCl structure. From Fernández Guillermet and Grimvall [5].

Table I. Properties of Stable and Metastable Carbides of V and Mn

Compound	Structure (Pearson symbol)	n_e ($e \cdot a^{-1}$)	Ω ($10^{-30}\ m^3 \cdot a^{-1}$)	θ_S (K)	k_S ($N \cdot m^{-1}$)	E_S (Ry)	$-\Delta^0 H(298.15)$ [$kJ \cdot (mol\ of\ atoms)^{-1}$]
VC[a]	(cF8)	4.50	9.058[e]	745[i]	391	7.794	50.41[n]
"V_3C_2"[a]	(hR20)	4.60	10.254[f]	656[j]	350	7.578	51(±2)[o]
V_2C[a]	(hP3)	4.67	10.950[f]	603[j]	326	7.374	48(±2)[o]
V_7C_3[b]	(oP40)	4.70	10.75[g]	587[k]	324[k]	7.25[k]	36.5(±3)[p]
V_5C_2[b]	(mC28)	4.71	10.90[g]	577[k]	319[k]	7.20[k]	35.0(±3)[p]
V_3C[b]	(oP16)	4.75	11.15[g]	554[k]	310[k]	7.10[k]	30.5(±3)[p]
$V_{23}C_6$[b]	(cF116)	4.79	11.60[g]	526[k]	298[k]	7.00[k]	25.5(±3)[p]
MnC[b]	(cF8)	5.50	8.70[g]	622[l]	283[l]	5.50[l]	−6.3(±6)[l]
Mn_3C_2[b]	(c)	5.80	9.00[g]	544[l]	252[l]	5.00[l]	6.5(±2)[l]
Mn_2C[b]	(d)	6.00	9.70[g]	488[l]	225[l]	4.70[l]	9(±2)[l]
Mn_7C_3[a]	(oP40)	6.10	9.472[h]	479[m]	227	4.662	11.18[q]
Mn_5C_2[a]	(mC28)	6.14	9.642[h]	468[m]	222	4.613	10.98[q]
Mn_3C[a]	(oP16)	6.25	9.838[h]	440[m]	207	4.36	10.09[q]
$Mn_{23}C_6$[a]	(cF116)	6.38	10.355[h]	431[m]	212	4.62	10.62[q]

[a] Stable phase.
[b] Metastable phase.
[c] Unspecified structure, considered here as (hR20).
[d] Unspecified structure, considered here as (hP3).
[e] From lattice-parameter data in Ref. 40.
[f] From lattice-parameter data in Ref. 21.
[g] Estimated by interpolation in Ω vs n_e plots, as discussed in Refs. 5 and 31.
[h] From lattice-parameter data in Ref. 41.
[i] From Ref. 28.
[j] Present evaluation, from entropy values assessed in Ref. 10.
[k] Present estimate, discussed in Section 4.2.
[l] Estimated in Ref. 31.
[m] Evaluated in Ref. 5 from entropy values assessed in Ref. 9.
[n] From Ref. 42.
[o] Experimental, from Ref. 38.
[p] Present estimate, discussed in Section 4.3.
[q] From the thermodynamic description assessed in Ref. 9.

The E_S, k_S, and θ_S values for Mn_3C_2, V_7C_3, V_5C_2, V_3C, and $V_{23}C_6$, obtained from the correlation in Fig. 1a, are given in Table I. For comparison we present values for the stable carbides of V and for the stable and metastable carbides of Mn. θ_S for VC is from Ref. 28, whereas θ_S for V_2C and V_3C_2 were evaluated by us using entropy information from Ref. 10. θ_S of Mn_7C_3, Mn_5C_2, Mn_3C, and $Mn_{23}C_6$ was evaluated in Ref. 5 using entropy information from Ref. 9. θ_S for the MnC(cF8), NaCl-structure phase, and Mn_2C (hP3)-structure phase, which are metastable in the Mn–C system, were obtained in a recent study by Fernández Guillermet and Grimvall [31]. To check partly that the θ_S values estimated by us are reasonable, we plot in Figs. 2a and b the results in Table I versus the mole fraction x_{Me} of V and Mn in the carbide, respectively. We also plot θ_S for bcc V obtained in Ref. 30 from entropy data. θ_S for α-Mn was approximated as in Ref. 17, by using the θ value obtained in Ref. 32 from a study of X-ray intensity data. The present estimates for θ_S of V_7C_3, V_5C_2, V_3C, and $V_{23}C_6$ (open symbols) fit well the variation with composition suggested by the data points for stable V-carbides and bcc-V (filled

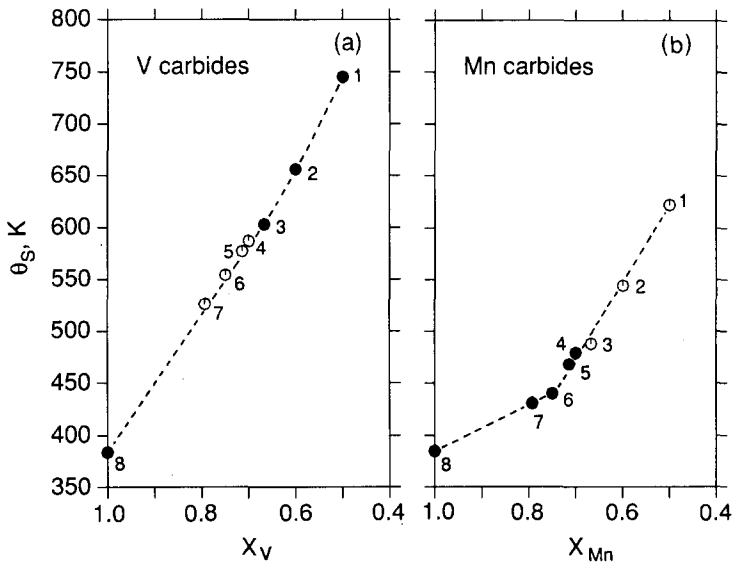

Fig. 2. The entropy Debye temperature θ_S of carbides as a function of the mole fraction of the metallic elements (x_{Me}) for (a) Me = V and (b) Me = Mn. Filled symbols represent θ_S values obtained from experimental or assessed entropy information, and open symbols represent estimated values. The dashed lines are to guide the eye. The numbers refer to MeC (1), Me_3C_2 (2), Me_2C (3), Me_7C_3 (4), Me_5C_2 (5), Me_3C (6), $Me_{23}C_6$ (7), and Me (8). The sources of information are given in Section 4.2.

symbols). Also, the result for Mn_3C_2 (open symbol labeled 2) fits well the trend of increasing θ_S with decreasing x_{Mn} suggested by the results for θ_S of Mn_3C, Mn_5C_2, and Mn_7C_3 (filled symbols labeled 6, 5, and 4, respectively) and the results for Mn_2C and MnC from Ref. 31 (open symbols labeled 3 and 1, respectively).

4.3. Estimation of Δ^0H for Metastable Carbides

The solid line in Fig. 1b gives a reasonably good description of the average variation with n_e of the (negative) enthalpy of formation of 3d-transition metal carbides at room temperature. Most of the carbides in Fig. 1b are stable phases in the metal–carbon phase diagram, and their properties have been studied experimentally. Fe_3C is a metastable phase in the Fe–C system, but its properties are known from experiments. Co_3C (oP16) and Ni_3C (oP16) are metastable, and information on their behavior has been obtained by extrapolating the properties of the $(Fe,Co)_3C$ and $(Fe,Ni)_3C$ ternary phases in the Co–Fe–C [33] and Fe–Ni–C [34] systems, respectively, using the two-sublattice model. A similar extrapolation is applied in Section 4.3.1 to gain information on $(-\Delta^0H)$ of V_3C (oP16). The estimation of $(-\Delta^0H)$ for the remaining carbides is discussed in Sections 4.3.2 and 4.3.3.

4.3.1. Treatment of the Metastable V_3C (oP16) Phase

Lacking experimental information on the stability of the $(Mn,V)_3C$ (oP16) phase, we estimate the $(-\Delta^0H)$ value for V_3C (oP16) by performing a model extrapolation of the data on another ternary phase, namely, $(Fe,V)_3C$. The properties of this phase have been dealt with by Huang in a recent assessment of the Fe–V–C system [35], but a different assumption about the entropy of V_3C (oP16) was adopted. In order to make the treatment of V_3C consistent with that of the other metastable carbides, we reanalyze here the experimental information considered by Huang [35] as follows.

The Gibbs energy of the $(Fe,V)_3C$ phase is expressed using Eqs. (8) and (11) as

$$G_m^{Me_3C} = y_{Fe}\,{}^0G_{Fe:C}^{Me_3C} + y_V\,{}^0G_{V:C}^{Me_3C} + bRT(y_{Fe}\ln y_{Fe} + y_V \ln y_V) + {}^EG_m^{Me_3C} \tag{20}$$

The parameter ${}^0G_{Fe:C}^{Me_3C}$, which describes the Gibbs energy of the Fe_3C (oP16) (cementite) phase, has been determined in Ref. 36 from

experiments. ${}^0G_{V:C}^{Me_3C}$ was expressed according to Eq. (10), and the function $\Delta^0G_{V_3C}(T)$ was represented by the equation

$$\Delta^0G_{V_3C}(T) = a + bT + cT\ln T + dT^{-2} \tag{21}$$

Parameters b, c, and d in Eq. (21) represent the temperature dependence of $\Delta^0G_{V_3C}(T)$ and of ${}^0G_{V:C}^{Me_3C}$, through Eq. (10), i.e., they describe the entropy function of the V_3C phase. They were determined by fitting to the entropy values obtained by inserting the predicted θ_S of V_3C (oP16) (Table I) in Eq. (19). The parameter a, which is related to the enthalpy of formation of V_3C, was determined by estimating the value of $(-\Delta^0H)$ at 298 K through an analysis of experimental data from Ref. 37 on the distribution of V between the $(Fe, V)_3C$ (oP16) phase and the fcc (cF4) phase in the Fe–V–C system, in the temperature range 1173 to 1373 K. In our analysis, the properties of the Fe–V–C fcc phase were taken from Ref. 35, whereas $(Fe, V)_3C$ was represented by Eq. (20) with ${}^0G_{Fe:C}^{Me_3C}$ from Ref. 36 and ${}^0G_{V:C}^{Me_3C}$ as before. Since the experimental data on $(Fe, V)_3C$ [37] considered by us involve the region of low V contents, we studied the effect on the extrapolation to V_3C of changes in the quantity ${}^0L_{Fe,V:C}^{Me_3C}$, which describes the interaction between Fe and V in the metallic sublattice of the $(Fe, V)_3C$ phase. We performed systematic fits to the experimental information from Ref. 37, for various choices of the ${}^0L_{Fe,V:C}^{Me_3C}$ parameter, and values of the enthalpy of formation of V_3C were determined which minimized the square sum of the difference between calculated and measured V contents in $(Fe, V)_3C$. The $(-\Delta^0H)$ value at 298 K which minimizes the error sum for a given ${}^0L$ is referred to as the "optimum" $(-\Delta^0H)$. The optimum $(-\Delta^0H)$ for V_3C and the corresponding error sum for each choice of ${}^0L_{Fe,V:C}^{Me_3C}$ are plotted in Fig. 3. Following a suggestion in Ref. 35 we refer ${}^0L_{Fe,V:C}^{Me_3C}$ to the quantity representing the interaction between Fe and V atoms in the Fe–V

Table II. Thermodynamic Parameters Obtained in the Present Work (in $J \cdot mol^{-1}$ of Formula Units)[a]

$${}^0G_{V:C}^{Me_3C} - 3H_V^{SER} - 1H_C^{SER} = -156971 + 601.922T - 100.438T\ln T + 765557T^{-1}$$

$${}^0G_{V:V:C}^{Me_{23}C_6} - 20H_V^{SER} - 3H_V^{SER} - 6H_C^{SER} = -990367 + 4330.63T - 728.83T\ln T + 5003425T^{-1}$$

$${}^0G_{V:C}^{Me_5C_2} - 5H_V^{SER} - 2H_C^{SER} = -307123 + 1059.7T - 175.66T\ln T + 1453274T^{-1}$$

$${}^0G_{V:C}^{Me_7C_3} - 7H_V^{SER} - 3H_C^{SER} = -454245 + 1518.48T - 250.981T\ln T + 2148692T^{-1}$$

$${}^0G_{Mn:C}^{Me_3C_2} - 3H_{Mn}^{SER} - 2H_C^{SER} = -76135 + 750.415T - 125.589T\ln T + 922711T^{-1}$$

[a] The thermodynamic descriptions of the binary systems Mn–C, V–C, and Mn–V are from Refs. 9, 10, and 11, respectively.

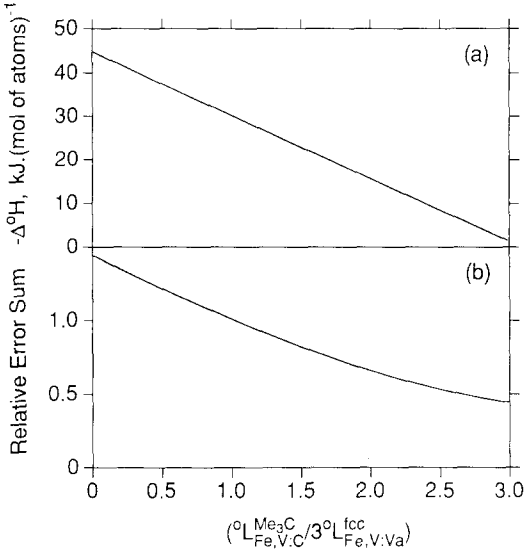

Fig. 3. (a) The "optimum" value of the negative enthalpy of formation of the metastable V_3C(oP16) carbide, defined in Section 4.3.1, and (b) the "relative" error sum (Section 4.3.1) describing the goodness of fit to experimental data [37] on the distribution of V between fcc and the $(Fe, V)_3C$ phase, for various choices of the phenomenological interaction parameter ${}^0L^{Me_3C}_{Fe,V:C}$. In these fits the interaction parameter ${}^0L^{fcc}_{Fe,V:Va}$ was given the value assessed by Huang [35].

fcc phase, ${}^0L^{fcc}_{Fe,V:Va}$, which we multiply by 3 to account for the difference in the number of metallic atoms per formula unit. Further, we refer the "optimum" error sum corresponding to a given $({}^0L^{Me_3C}/3\,{}^0L^{fcc})$ ratio to the error sum obtained when the ratio was set equal to unity and called this ratio the "relative" error sum.

It is evident from Fig. 3b that the goodness of fit decreases with a decrease in the $({}^0L^{Me_3C}/3\,{}^0L^{fcc})$ ratio, whereas the optimum $(-\Delta^0H)$ increases (Fig. 3a). However, phase diagram calculations performed by combining the description of the V–C system from Ref. 10 with a description of V_3C based on the optimum $(-\Delta^0H)$ and the entropy from our predicted θ_S (Section 4.2) showed that increasing $(-\Delta^0H)$ above 37.7 kJ · (mol of atom)$^{-1}$ makes V_3C (oP16) a stable phase in the V–C phase diagram, which is against experiments. Therefore the value $(-\Delta^0H) = 37.7$ kJ · (mol of atoms)$^{-1}$ was taken as an upper limit of the

probable $(-\Delta^0 H)$ of V_3C at 298.15 K. It can be seen from Fig. 3 that optimum $(-\Delta^0 H)$ values compatible with that limit can be obtained from the experimental data in Ref. 37 only if the interactions between the Fe and V atoms in fcc and in $(Fe, V)_3C$ are comparable, say, if ${}^0L^{Me_3C}/3\,{}^0L^{fcc} \geqslant 0.5$. On the other hand, a sufficiently large increase in the ${}^0L^{Me_3C}/3\,{}^0L^{fcc}$ ratio would lead to very small $(-\Delta^0 H)$ "optimum" values, which will, in general, mean a decrease in the strength of the chemical bonding in V_3C. However, that decrease would not be in line with the large θ_S and effective force constant k_S expected for this carbide from the correlation in Fig. 1a. As a consequence, an intermediate ${}^0L^{Me_3C}/3\,{}^0L^{fcc}$ value was preferred when estimating the probable $(-\Delta^0 H)$ for V_3C. Lacking further information, we adopted as a probable enthalpy of formation, the "optimum" $(-\Delta^0 H)$ extracted from experiments under the assumption that $({}^0L^{Me_3C}_{Fe,V:C}/{}^0L^{fcc}_{Fe,V:V_a}) = 1$. We obtained $(-\Delta^0 H) = 30.5(\pm 3)$ kJ · (mol of atoms)$^{-1}$ and could thus evaluate the whole $\Delta^0 G_{V_3C}(T)$ expression; see Table II. To be consistent, the new expression for V_3C is also adopted in the Fe–V–C system, which was previously described with a value of $(-\Delta^0 H) = 24.0$ kJ · (mol of atoms)$^{-1}$ at 298 K. The new value does not result in any appreciable change in the Fe–V–C system, since both analyses are based on the same experimental information by Ohtani [37]. Another estimate for $(-\Delta^0 H)$ of V_3C is available from the approach developed by Miedema and co-workers [4]. It is considered in the following section.

4.3.2. *Treatment of V_7C_3, V_5C_2, and $V_{23}C_6$*

Once the $(-\Delta^0 H)$ for the metastable V_3C (oP16) carbide was determined, we performed interpolations in a $(-\Delta^0 H)$ versus n_e plot and estimated the values for the remaining metastable V carbides. The interpolations were based on the observation [31] that the $(-\Delta^0 H)$ values for the various stable complex carbides of Cr (i.e., Cr_3C_2, Cr_7C_3, and $Cr_{23}C_6$) and Mn (i.e., Mn_7C_3, Mn_5C_2, Mn_3C and $Mn_{23}C_6$) are roughly represented by the straight line in a $(-\Delta^0 H)$ versus n_e plot, which goes through the point corresponding to pure Cr (i.e., $\Delta^0 H = 0$, $n_e^{Cr} = 6e \cdot a^{-1}$) and pure Mn (i.e., $\Delta^0 H = 0$, $n_e^{Mn} = 7e \cdot a^{-1}$), respectively. In the present case, the $(-\Delta^0 H)$ versus n_e value for V_3C from Section 4.3.1 fits fairly well the linear variation determined by the experimental [38] $(-\Delta^0 H)$ for V_3C_2 $(n_e = 4.60e \cdot a^{-1})$ and the values representing pure V (i.e., $\Delta^0 H = 0$, $n_e^V = 5e \cdot a^{-1}$). Interpolations of $(-\Delta^0 H)$ based on that linear variation yield 36.5 (± 3) kJ · (mol of atoms)$^{-1}$ for V_7C_3, 35.0 (± 3) kJ · (mol of atoms)$^{-1}$ for V_5C_2, and 25.5 (± 3) kJ · (mol of atoms)$^{-1}$ for $V_{23}C_6$. In Fig. 4 we plot n_e versus the $(-\Delta^0 H)$ values for metastable carbides (open symbols) obtained by us, the experimental [38] $(-\Delta^0 H)$ of

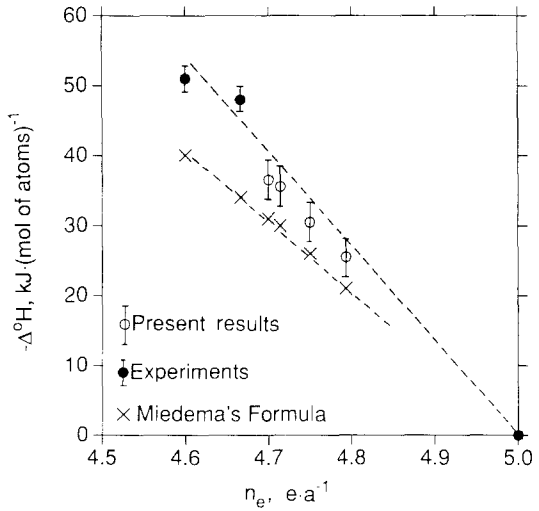

Fig. 4. The negative enthalpy of formation of complex carbides of V at 298.15 K $(-\Delta^0 H)$ as a function of the average number of valence electrons per atom, n_e. Filled symbols represent experimental values for V_3C_2 and V_2C from Ref. 38. The filled symbol placed at $(-\Delta^0 H) = 0$, $n_e^V = 5e \cdot a^{-1}$ represents bcc V at 298.15 K. Open symbols represent the results for V_7C_3, V_5C_2, V_3C, and $V_{23}C_6$ obtained in Sections 4.3.1 and 4.3.2, and the error bars represent our estimates of the probable uncertainty. Crosses represent the values given by Miedema and co-workers' [4] formula. The dashed lines are to guide the eye.

V_3C_2 and V_2C (filled symbols), and the values given by Miedema and co-workers' [4] formula (crosses). There is fair agreement between our results for the metastable V carbides and those from Ref. 4, although our $(-\Delta^0 H)$ are larger. This systematic difference seems to be consistent with the fact that Miedema and co-workers' [4] formula also gives for V_3C_2 and V_2C $(-\Delta^0 H)$ values which are smaller than the experimental data from [38]; see Fig. 4.

4.3.3. Treatment of the Metastable Mn_3C_2 Carbide

It has been noted [5] that the data points representing $(-\Delta^0 H)$ for the stable Mn carbides fall above the solid line in Fig. 1a, and a similar type of deviation has been observed in an analysis of 3d-transition metal nitrides (see Fig. 6 in Ref. 5). These deviations from the general trends have

qualitatively been explained [5] in terms of the anomalously low cohesive energy of α-Mn. Although a quantitative treatment of the anomaly has not yet been developed, it is expected that the magnitude of the anomalous effect will be less for Mn_3C_2 than for the stable Mn carbides, which have a larger Mn content. Relying on this expectation, the enthalpy of formation of a carbide with the formula Mn_3C_2 and unspecified structure has tentatively been estimated in Ref. 31, by making use of the solid line in Fig. 1b. That result, which is $(-\Delta^0 H) = 6.5(\pm 2)$ kJ · (mol of atoms)$^{-1}$, was adopted by us to treat the metastable Mn_3C_2 (hR20) carbide.

4.4. Representation of Lattice Stabilities

The enthalpy of formation values for metastable carbides obtained by us (Table I) were combined with entropy values calculated by inserting the estimated θ_S (Table I) in Eq. (19), and the Gibbs energy functions ${}^0G^{Me_3C_2}_{Mn:C}$, ${}^0G^{Me_3C}_{V:C}$, ${}^0G^{Me_7C_3}_{V:C}$, ${}^0G^{Me_5C_2}_{V:C}$, and ${}^0G^{Me_{23}C_6}_{V:C}$ were determined, by fitting the temperature-dependent quantities $\Delta^0 G_{Mn_3C_2}$ [Eq. (9)] and $\Delta^0 G_{V_bC_C}$ [Eqs. (10), (13)] to the four-parameter function of T given in Eq. (21). All lattice-stability parameters obtained in the present work are given in Table II.

5. EXCESS GIBBS ENERGY OF CARBIDE PHASES

The Gibbs energy function of the fcc phase and the MeC (cF8) carbide, and of the hcp phase and the hexagonal Me_2C (hP3) carbide, expressed by Eqs. (1) and (2) involves quantities originated in the lower-order systems and, in addition, the excess Gibbs energy parameters ${}^0L^{fcc}_{Mn,V:C}$ and ${}^0L^{hcp}_{Mn,V:C}$, respectively. They account phenomenologically for the interaction between the atoms of Mn and V in the metallic sublattice of the $(Mn, V)_1 C_1$ and $(Mn, V)_1 C_{0.5}$ carbide, respectively, which is, in principle, to be determined from ternary experimental data. Furthermore, phenomenological interaction parameters remain to be determined for the carbide phases $(Mn, V)_3 C_2$, $(Mn, V)_7 C_3$, $(Mn, V)_5 C_2$, $(Mn, V)_3 C$, and $(Mn, V)_{20}(Mn, V)_3 C_6$, the Gibbs energy of which are described by Eqs. (8), (11), and (12). Lacking ternary information, the interaction between Mn and V atoms in the carbide phases was determined by comparison with that in the Mn–V binary system, in line with our analysis of the $(Fe, V)_3 C$ phase, Section 4.3.1. Two possible assumptions were tested. First, we assumed that the interaction parameter per atom of the metallic sublattice of all carbide phases is comparable to that in the solid solution phases of the Mn–V system, which is of the order of -10 kJ · (mol of atoms)$^{-1}$ according to Ref. 11. Second, we assumed that the interaction

parameter in the metallic sublattice of all carbide phases was equal to zero. Calculations of the Mn–V–C phase diagram performed by us indicated that the first assumption leads to a stabilization of the hexagonal carbide phase which is larger than expected from a consideration of the ternary systems formed by replacing Mn for the neighboring elements in the 3d-metal row of the periodic table, viz., the Cr–V–C and Fe–V–C systems; see Section 6.2. This was taken as an indication that the first assumption overestimates the negative deviations from ideality in the hexagonal carbide phase, and thus the second, more conservative assumption was preferred for this phase. Lacking further information, the second assumption was adopted for the cubic carbide and the complex carbides as well. The phase diagram calculations reported in the remainder of the present paper were performed by setting equal to zero the parameters describing the excess Gibbs energy of the mixture of Mn and V atoms in the metallic sublattice of all carbide phases.

6. THE PREDICTED Mn–V–C PHASE DIAGRAM

6.1. Isothermal Sections

The thermodynamic parameters of the Mn–V–C system arrived at in the present study are given in Table II. In Figs. 5, 6, and 7 we present the

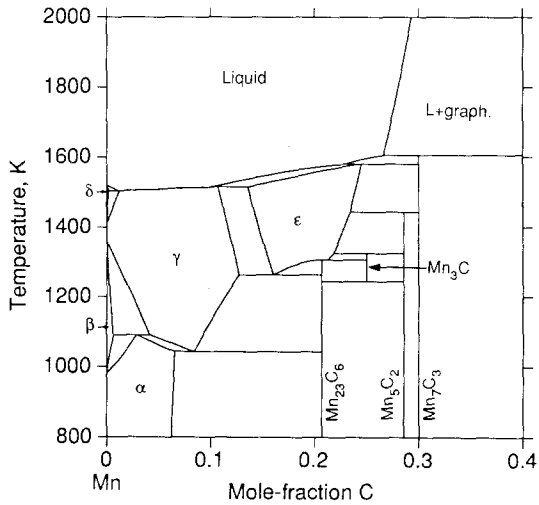

Fig. 5. The Mn–C phase diagram calculated using the thermodynamic description assessed by Huang [9], used as a basis for the present work.

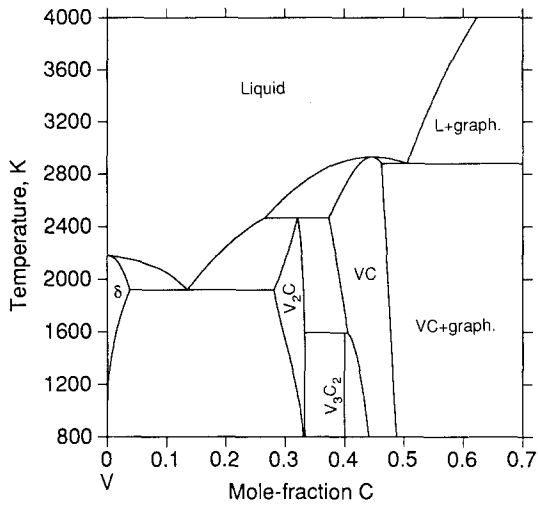

Fig. 6. The V–C phase diagram calculated using the thermodynamic description assessed by Huang [10], used as a basis for the present work.

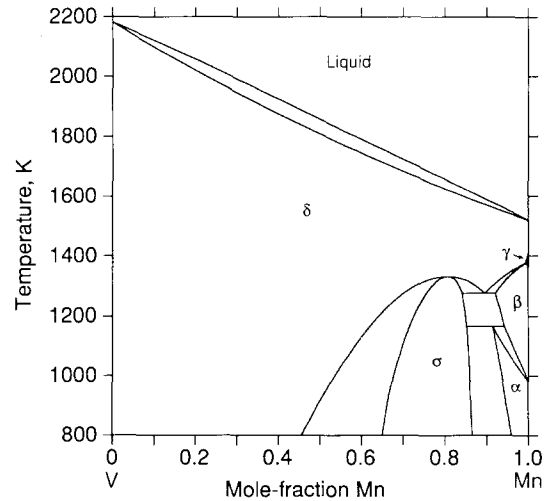

Fig. 7. The Mn–V phase diagram calculated using the thermodynamic description assessed by Huang [11], used as a basis for the present work.

Mn–C, V–C, and Mn–V phase diagram, respectively, calculated using the thermodynamic descriptions assessed by Huang, Refs. 9, 10, and 11, which form the basis of the present treatment of the Mn–V–C system. According to Fig. 5, the carbides $Mn_{23}C_6$, Mn_5C_2, and Mn_7C_3 are stable at the Mn–C side of the ternary system at 1000 K, whereas the hexagonal (V_2C), the cubic (VC), and the V_3C_2 carbides are the stable ones on the V–C side (Fig. 6). In Fig. 8 we present the isothermal section of the Mn–V–C phase diagram calculated at 1000 K using the present thermodynamic description. The experimental information on the extension of these carbide phases into

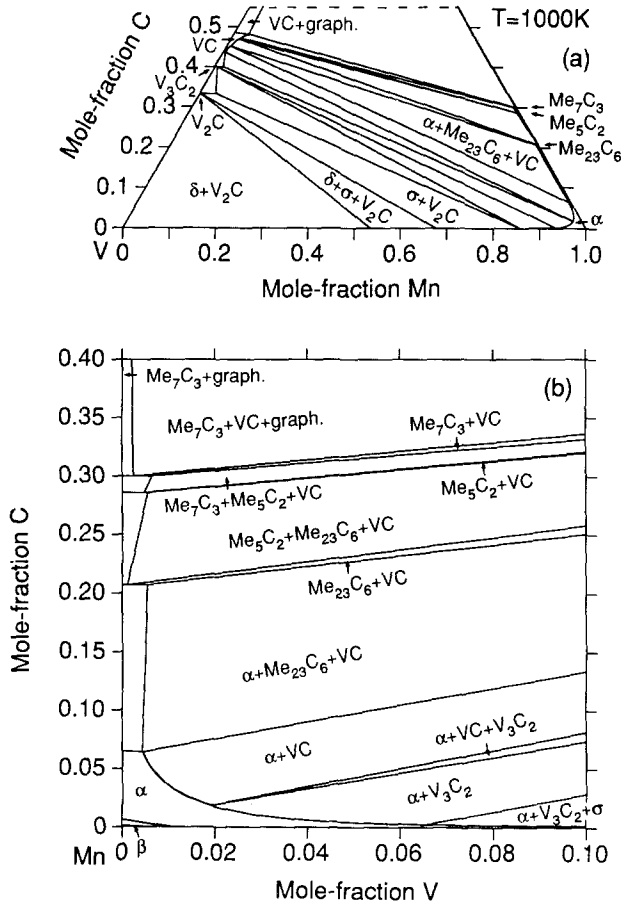

Fig. 8. (a) The isothermal section and (b) an enlargement of the Mn-rich corner of the Mn–V–C phase diagram at 1000 K, calculated using the present thermodynamic description; see Table II.

the ternary system is not available, and our treatment predicts at 1000 K relatively small solubilities of Mn in the V carbides and of V in the Mn carbides (Fig. 8b). The effect of temperature upon the maximum solid solubilities may be examined by comparing Fig. 8 with the results of a calculation from 1230 K (Fig. 9). There is a small increase in the calculated solubility of the various carbide phases, for instance, the carbides of Mn are predicted to dissolve up to about 1 atomic % of V (Fig. 9b).

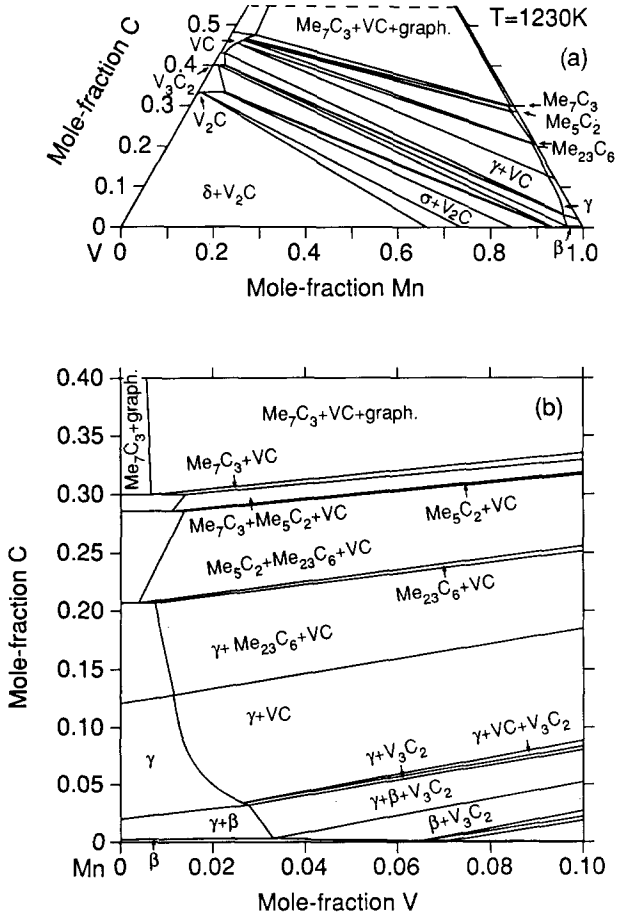

Fig. 9. (a) The isothermal section and (b) an enlargement of the Mn-rich corner of the Mn–V–C phase diagram at 1230 K, calculated using the present thermodynamic description; see Table II.

6.2. Qualitative Comparisons with Related Systems

In this section we consider the phase equilibria in the Mn–V–C system at higher temperatures and compare our results with information on the related system Fe–V–C, recently assessed by Huang [35]. High-temperature solid–solid phase equilibria are considered in Fig. 10. There we compare the isothermal section of the Mn–V–C (Fig. 10a) phase diagram calculated at 1400 K using the present thermodynamic description with the corresponding section of Fe–V–C system (Fig. 10b) using the description assessed in Ref. 35. There is a general similarity between these diagrams, but a difference is observed in the extension of the cubic and hexagonal carbide phase into the ternary Me–V–C system, which decreases when Me moves from Mn to Fe. This effect may qualitatively be related to the observation from Ref. 31 of a general decrease in properties related to the stability of various binary MeC (cF8) and Me_2C (hP3) 3d-transition metal carbides with the increase in the average number of valence electrons per

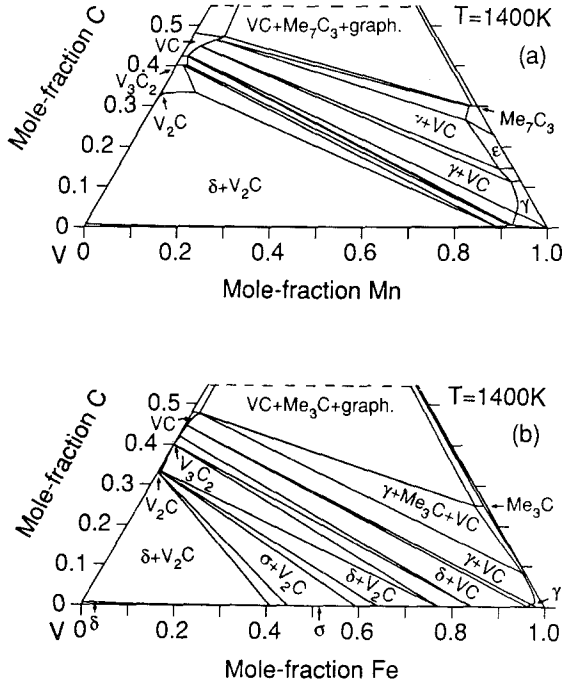

Fig. 10. Isothermal section at 1400 K of (a) the Mn–V–C phase diagram according to the present thermodynamic description (see Table II) and (b) the Fe–V–C phase diagram according to the description assessed by Huang [35].

atom in the carbide, when Me = Ti to Ni. The decrease in stability of the ternary (Me, V) C and $(Me, V)_2$ C phases associated to the change from Me = Mn ($n_e = 7e \cdot a^{-1}$) to Fe ($n_e = 8e \cdot a^{-1}$) is in line with that observation. Following the same trend one would expect an increase in the stability of those ternary carbide structures when moving from the Mn–V–C to the Cr–V–C system. The lack of information on the Cr–V–C phase diagram precludes a direct comparison with our results on the Mn–V–C system at 1400 K. However, a Cr–V–C isothermal section from a higher temperature, 1623 K, presented by Kieffer and Rassaerts [39], shows one-phase fields for the cubic and hexagonal carbides extending into the ternary system considerably more than in the Mn–V–C case, which is also in line with the trend noted in Ref. 31. Finally, we present in Fig. 11a the calculated projection of the liquidus surface for

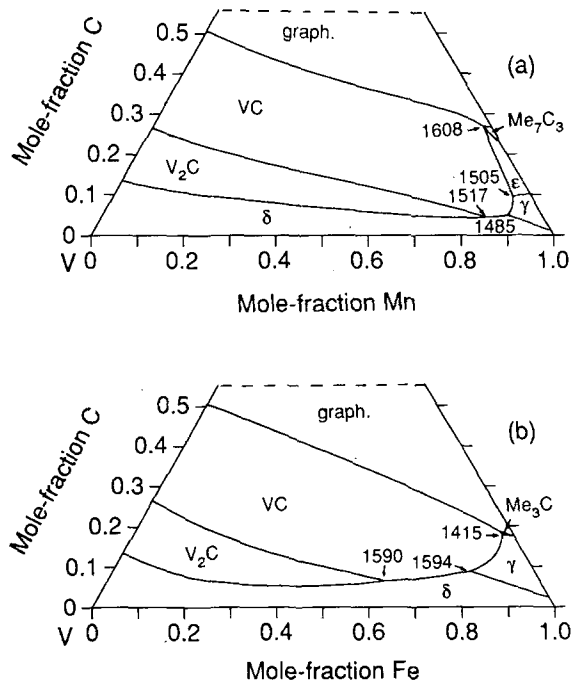

Fig. 11. Projection of the liquidus surface of (a) the Mn–V–C system, according to the present thermodynamic description (see Table II) and (b) the Fe–V–C system, according to the description assessed by Huang [35]. The solid lines indicate the composition of the liquid phase in equilibrium with two solid phases. All temperature values are given in K.

the Mn–V–C system. Our calculation indicates for the Mn–V–C system a liquidus surface resembling that reported in Ref. 35 for the Fe–V–C system, which is reproduced in Fig. 11b.

7. SUMMARY

The thermodynamics of the Mn–V–C system is not known from experiments, and there is a need for guidelines in estimating the thermodynamic properties and stability of the various phases and constructing a probable phase diagram. In the present paper we have presented a possible approach to this problem, based on constructing probable Gibbs energy functions for the various phases. The key idea of our treatment of the carbides is to apply a phenomenological model for Gibbs energy of interstitial phases, the so-called "two-sublattice" model, and to predict the unknown model parameters. Our predictions rely on regularities in the effect of the number of valence electrons per atom upon the bonding properties and the vibrational entropy of 3d-transition metal carbides. The Mn–V–C phase diagram predicted by us accounts for the substitution of Mn for V in all carbide phases and fits well the trends of the information on related systems.

ACKNOWLEDGMENTS

We like to thank Professor Mats Hillert for his valuable comments on this paper. One of us (A.F.G.) also acknowledges the benefits of many discussions with Professor Göran Grimvall. This research was partly supported by the Swedish Board for Technical Development.

REFERENCES

1. L. Kaufman and H. Bernstein, *Computer Calculation of Phase Diagrams* (Academic Press, New York, 1970).
2. See also the *Calphad Journal*, Pergamon Press, Oxford.
3. J.-O. Andersson, A. Fernández Guillermet, M. Hillert, B. Jansson, and B. Sundman, *Acta Metall.* **34**:437 (1986).
4. F. R. de Boer, R. Boom, W. C. M. Matterns, A. R. Miedema, and A. K. Niessen, *Cohesion in Metals* (North-Holland, Amsterdam, 1988).
5. A. Fernández Guillermet and G. Grimvall, *Phys. Rev. B* **40**:10582 (1989).
6. A. Fernández Guillermet and G. Grimvall, *Z. Metallkunde* **81**:521 (1990).
7. A. Fernández Guillermet and K. Frisk, *Int. J. Thermophys.* **12**:417 (1991).
8. A. Fernández Guillermet, *Int. J. Thermophys.* **12**:919 (1991).
9. W. Huang, *Scand. J. Metall.* **10**:26 (1990).
10. W. Huang, *Z. Metallkunde* **82**:174 (1991).
11. W. Huang, *Calphad* **15** (1991), in press.

12. M. Hillert and M. Jarl, *Calphad* **2**:227 (1978).
13. G. Inden, *Project Meeting Calphad V*, (Düsseldorf, Max Planck Institute Eisenforsch, 1976), pp. 1–13.
14. M. Hillert and L.-I. Staffansson, *Acta Chem. Scand.* **24**:3618 (1970).
15. B. Sundman and J. Ågren, *J. Phys. Chem. Solids* **42**:297 (1981).
16. M. Hillert, in *Computer Modeling of Phase Diagrams*, L. H. Bennett, ed. (Metallurgical Society, Warrendale, 1986).
17. A. Fernández Guillermet and W. Huang, *Int. J. Thermophys.* **11**:949 (1990).
18. Scientific Group Thermodata Europe (SGTE) Data for Pure Elements, Compiled by A. T. Dinsdale, NPL Report DMA(A) 195 (National Physics Laboratory, Teddington, UK, 1989).
19. A. Fernández Guillermet and W. Huang, *Z. Metallkunde* **79**:88 (1988).
20. O. Redlich and A. T. Kister, *Ind. Eng. Chem.* **40**:345 (1948).
21. O. N. Carlson, A. H. Ghaneya, and J. F. Smith, *Bull. Alloy Phase Diagrams* **6**:115 (1985).
22. P. Gustafson, *Carbon* **24**:169 (1986).
23. J.-O. Andersson, *Metall. Trans.* **19A**:627 (1988).
24. P. Gustafson, *Metall. Trans.* **19A**:2547 (1988).
25. J.-O. Andersson, *Trita-Mac-0323* (Royal Institute of Technology, Stockholm, Sweden, 1986).
26. B. Jansson, Ph.D. thesis (Division of Physical Metallurgy, Royal Institute of Technology, Stockholm, Sweden).
27. A. Fernández Guillermet and M. Hillert, *Calphad* **12**:337 (1988).
28. G. Grimvall and J. Rosén, *Int. J. Thermophys.* **4**:139 (1983).
29. J. Rosén and G. Grimvall, *Phys. Rev. B* **27**:7199 (1983).
30. A. Fernández Guillermet and G. Grimvall, *Phys. Rev. B* **40**:1521 (1989).
31. A. Fernández Guillermet and G. Grimvall, *J. Phys. Chem. Solids*, accepted for publication, (1991).
32. C. P. Gazzara, R. M. Middleton, and R. J. Weiss, *Phys. Lett.* **10**:257 (1964).
33. A. Fernández Guillermet, *Z. Metallkunde* **79**:317 (1988).
34. A. Gabriel, P. Gustafson, and I. Ansara, *Calphad* **11**:203 (1987).
35. W. Huang, *Z. Metallkunde* **82**:391 (1991).
36. P. Gustafson, *Scand. J. Metall.* **14**:259 (1985).
37. H. Ohtani, Private communication, Faculty of Engineering, Tohoku University, Sendai, Japan.
38. N. M. Volkova and P. V. Gel'd, *Izv. VUZ. Tsvetn. Metall.* **8**:77 (1965).
39. R. Kieffer and H. Rassaerts, *Metallwiss. Technik* **20**:691 (1966).
40. P. Zhukov, V. A. Gubanov, O. Jepsen, N. E. Christensen, and O. K. Andersen, *J. Phys. Chem. Solids* **49**:841 (1988).
41. P. Villars and L. D. Calvert, *Pearson's Handbook of Crystallographic Data for Intermetallic Phases* (American Society for Metals, Metals Park, OH, 1985).
42. O. Kubaschewski and C. B. Alcock, *Metallurgical Thermochemistry*, 5th ed. (Pergamon, Oxford, 1979).